JOURNAL OF NEUROTRAUMA 31:1998–2002 (December 15, 2014)

DOI: 10.1089/neu.2014.3349

Short Communication

Assessment of White Matter Loss Using Bond-Selective Photoacoustic Imaging in a Rat Model of Contusive Spinal Cord Injury

Wei Wu,[1,2,*] Pu Wang,[2,*] Ji-Xin Cheng,[2] and Xiao-Ming Xu[1]

Abstract

White matter (WM) loss is a critical event after spinal cord injury (SCI). Conventionally, such loss has been measured with histological and histochemical approaches, although the procedures are complex and may cause artifact. Recently, coherent Raman microscopy has been proven to be an emerging technology to study de- and remyelination of the injured spinal cord; however, limited penetration depth and small imaging field prevent it from comprehensive assessments of large areas of damaged tissues. Here, we report the use of bond-selective photoacoustic (PA) imaging with 1730-nm excitation, where the first overtone vibration of CH_2 bond is located, to assess WM loss after a contusive SCI in adult rats. By employing the first overtone vibration of CH_2 bond as the contrast, the mapping of the WM in an intact spinal cord was achieved in a label-free three-dimensional manner, and the physiological change of the spinal cord before and after injury was observed. Moreover, the recovery of the spinal cord from contusive injury with the treatment of a neuroprotective nanomedicine ferulic-acid–conjugated glycol chitosan (FA-GC) was also observed. Our study suggests that bond-selective PA imaging is a valuable tool to assess the progression of WM pathology after SCI as well as neuroprotective therapeutics in a label-free manner.

Key words: deep tissue imaging; photoacoustic imaging; spinal cord injury; white matter loss

Introduction

EXCLUDING THE DEATH at the scene of an accident, the annual incidence of spinal cord injury (SCI) is approximately 12,000 new cases per year in the United States, causing tetra- or paraplegia according to the reports of the National Spinal Cord Injury Statistical Center. The pathological progression after SCI includes two phases: a primary injury, followed by a much more complicated secondary injury. The primary injury is a mechanical injury to the spinal cord, which mainly leads to gray matter (GM) damage. The secondary injury, induced by multiple injury insults, such as inflammation, glutamate excitotoxicity, and oxidative stress, spreads out the damage to white matter (WM), leading to WM loss. Clinically, because the damage to the GM is fast, the repairing of the GM at the injury site, which is directly damaged by the mechanical force, is difficult to achieve.[1] Nevertheless, it has been reported that the WM could be rescued and recover its function to a certain extent by multiple means, including sodium channel blocker tetrodotoxin or glutamate receptor antagonism NBQX.[2–4] The development of those therapeutic strategies raises the demand for feasible and reliable methods to monitor WM damage and repair in a longitudinal fashion.

Traditionally, histology and immunohistochemistry were widely used to assess WM pathology through complex staining procedures using specific antibodies, such as SMI-31 for axons, ionized calcium binding adaptor molecule 1 for microglia, glial fibrillary acidic protein for astrocytes, or chemicals such as the Luxol fast blue for myelin sheath.[5,6] All those techniques can be used to observe morphology changes of various types of cells or structures in the WM at the cellular level. However, the requirement of the staining procedure may cause false outcomes[7,8]. Moreover, because tissue sectioning is needed, *in vivo* assessment of the WM loss is formidable. Recently, *in vivo* observation of injury progression of the spinal cord has been achieved by using the multiphoton microscopy technique on transgenic animals expressing fluorescence proteins.[9] However, genetically engineered genes may affect the physiology of the spinal cord. Previously, we demonstrated that coherent anti-Stokes Raman scattering (CARS) microscopy can be used to observe de- and remyelination in the spinal cord in a label-free manner.[10,11] Although CARS offers

[1]Spinal Cord and Brain Injury Research Group, Stark Neurosciences Research Institute, Department of Neurological Surgery, Goldman and Campbell Brain and Spine, Indiana University School of Medicine, Indianapolis, Indiana.
[2]Weldon School of Biomedical Engineering, Purdue University, West Lafayette, Indiana.
*The first two authors contributed equally.

chemically selective imaging of WM with high sensitivity and submicron resolution, it suffers from shallow penetration depth in the spinal cord ($\sim 100\,\mu$m) and the limited field of view (less than 1 mm^2), limiting its use for assessing global WM injury and repair in animal models.

Photoacoustic (PA) imaging of vibrationally excited molecules offers a unique opportunity to overcome limitations discussed above.[12,13]. This method uses pulsed laser excitation of overtone transitions in target molecules inside a tissue. The absorption of the photons leads to local temperature rise and thus generating acoustic waves, which are detectable by an ultrasonic transducer. This method maintains the chemical selectivity as a result of the contrast of molecular vibration, with gains in the imaging depth owing to the fact that the attenuation of acoustic wave in biological tissue is considered much lower than that of light.[14]

In the present study, we report on PA imaging of the spinal cord using 1730-nm excitation, which is the first overtone absorption peak of CH_2 vibration. We demonstrate that the WM provides 2 times higher contrast than the GM owing to the abundant CH_2 bonds presenting in myelin sheath. Three-dimensional (3D) PA imaging of the healthy, injured, and recovered spinal cords indicates that bond-selective PA imaging can be applied for assessing WM damage and repair. This development opens up a new opportunity for *in vivo* assessments of injury progression as well as interventional therapies.

Methods

All animal use protocols were approved by the Purdue University Animal Use and Care Committee (West Lafayette, IN). Adult Long Evans rats (~ 300 g) were anesthetized with 90 mg/kg of ketamine and 5 mg/kg of xylazine. A T10 laminectomy was performed to expose the underlying thoracic spinal cord. Spinal cord contusion was produced using a weight-drop device developed at New York University (NYU model).[15] Briefly, the exposed dorsal surface of the cord was subjected to a weight-drop impact using a 10-g rod (2.5 mm in diameter) dropped from a height of 12.5 mm. After the injury, the muscles and skin were closed in layers, and rats were placed on a heating pad to maintain their body temperature until they awoke. Two hours after injury, ferulic-acid–conjugated glycol chitosan (FA-GC) nanomedicine in 1 mL of saline was given to rats by intravenous injection into the jugular vein. Both ferulic acid and glycol chitosan have neuroprotective effects, such as antioxidation and -inflammation.[16–22]. The analgesic, buprenorphine (0.05–0.10 mg/kg), was administered every 12 h through subcutaneous injection for the first 3 days postsurgery for postoperation pain management. Bladder expression was manually carried out 3 times a day until reflex bladder emptying was established. Because this study is a proof of concept, we did not conduct a quantification analysis, and 1 rat was used for each group.

Four weeks postinjury, animals were anesthetized and transcardially exsanguinated with 150 mL of physiological saline followed by fixation with 300 mL of ice-cold 4% paraformaldehyde (PFA) in phosphate-buffered saline (PBS; pH 7.4). A 1.5-cm thoracic spinal cord segment at the lesion center was dissected and then fixed for 4 h by 4% PFA in PBS (PH 7.4) and transferred to 30% sucrose in PBS (pH 7.4). For cross-sectional imaging, spinal cord tissue was sectioned at 80 μm, transferred into heavy water (D_2O) for 5 min, and then was placed in a glass-bottomed dish and embedded in D_2O agarose gel.

As shown in Figure 1, a Nd:YAG pumped optical parametric oscillator (OPO; Panther® Ex Plus; Continuum, Santa Clara, CA) was used as the excitation source. The excitation module provides 10-Hz, 5-ns pulses laser with the wavelength range from 400 up to 2500 nm. The near-infrared light, produced at the idler beam from the OPO, was directed to an inverted microscope (IX-71; Olympus, Tokyo, Japan) for spectroscopy and imaging purposes. The laser irradiation was focused by an achromatic doublet lens (30-mm focal length; Thorlabs, Inc., Newton, NJ). A focused-type, 20-MHz ultrasound transducer with a 50% bandwidth (V317; Olympus NDT) was employed to detect the PA signal. A 30-dB low-noise preamplifier (5682; Olympus NDT Inc., Waltham, MA) and a receiver (5073PR-15-U; Olympus NDT) with adjustable gain were applied for receiving signal. The signal was then sent to a digitizer (USB-5133; National Instruments Corporation, Austin, TX), recorded by personal computer (PC) by a LabVIEW (National Instruments) program. PA spectra were taken by automatic laser wavelength scanning of the OPO system. For the 3D PA imaging, a two-dimensional (2D) scanning stage (ProScan H117; Prior Scientific, Inc., Rockland, MA) was employed for the raster scanning. All 2D images were reconstructed using a MATLAB program (The MathWorks, Inc., Natick, MA), while 3D images and movies were built by ImageJ (National Institutes of Health [NIH], Bethesda, MD).

Results and Discussion

To compare the PA image with histology, Luxol fast blue (LFB) staining was used to observe myelin in the spinal cord according to a previously published protocol.[23] Cross-sections of the injured spinal cord were dehydrated with 70% and 95% alcohol for 2 min each and then were immersed with 0.1% LFB solution at 37°C for 4 h. After cooling at 4°C for 20 min, the slides were dipped in 95% alcohol 5 times and dH_2O for 1 min and then were cleared and cover-slipped.

PA spectroscopy and imaging were first performed to determine its ability to characterize the histology of a normal rat spinal cord. In order to determine the optimal wavelength for PA imaging of the WM, we first recorded PA spectra of the extracted spinal cord (Fig. 2A). It is shown that the spectrum of CH_2-riched WM has two peaks located at 1730 nm for the first overtone and 1200 nm for the second overtone of CH_2 vibration. The amplitude of the signal at 1730 nm is 5.8 times higher than that at 1200 nm, which is consistent with the results of our previous study.[12] We then performed a C-scan PA imaging of a cross-sectional slide of a rat spinal cord (Fig. 2B) to exam the contrast deference between the WM and GM under 1730 nm excitation at 15 mJ per pulse. It has been shown that the contrast between the WM and GM is 2.25:1, likely caused by the presence of a large number of CH_2 bonds in myelinated axons in the WM. We performed B-scan mode PA imaging of fixed intact spinal cord under 1730-nm excitation. As shown in Figure 2C, the penetration depth of the WM was $\sim 200\,\mu$m, whereas the penetration depth increased to ~ 1.3 mm at the dorsolateral surface of the cord above the dorsal horn (Fig. 2B,C, red arrows). It is known that the WM has a higher scattering coefficient (296 cm^{-1} at 1064 nm) than that of GM (57 cm^{-1} at 1064 nm).[24] Therefore, the penetration difference is mainly caused by the scattering coefficient difference between the WM and GM. These results have suggested that the high PA contrast and high scatter coefficient represent a unique feature of WM in PA images, allowing us to examine WM morphology and changes in the normal and injured spinal cords.

Next, PA imaging of normal and injured spinal cords was compared to determine whether PA is a sensitive measure of pathological changes between these spinal cords (Fig. 2D,E). Moreover, a neuroprotective treatment with FA-GC was evaluated to determine whether PA imaging is sensitive for assessing the neuroprotective effect of a treatment agent (Fig. 2F). Rats in the control and treatment groups received saline and FA-GC, respectively, after the contusive SCI. Spinal cords were harvested at 28

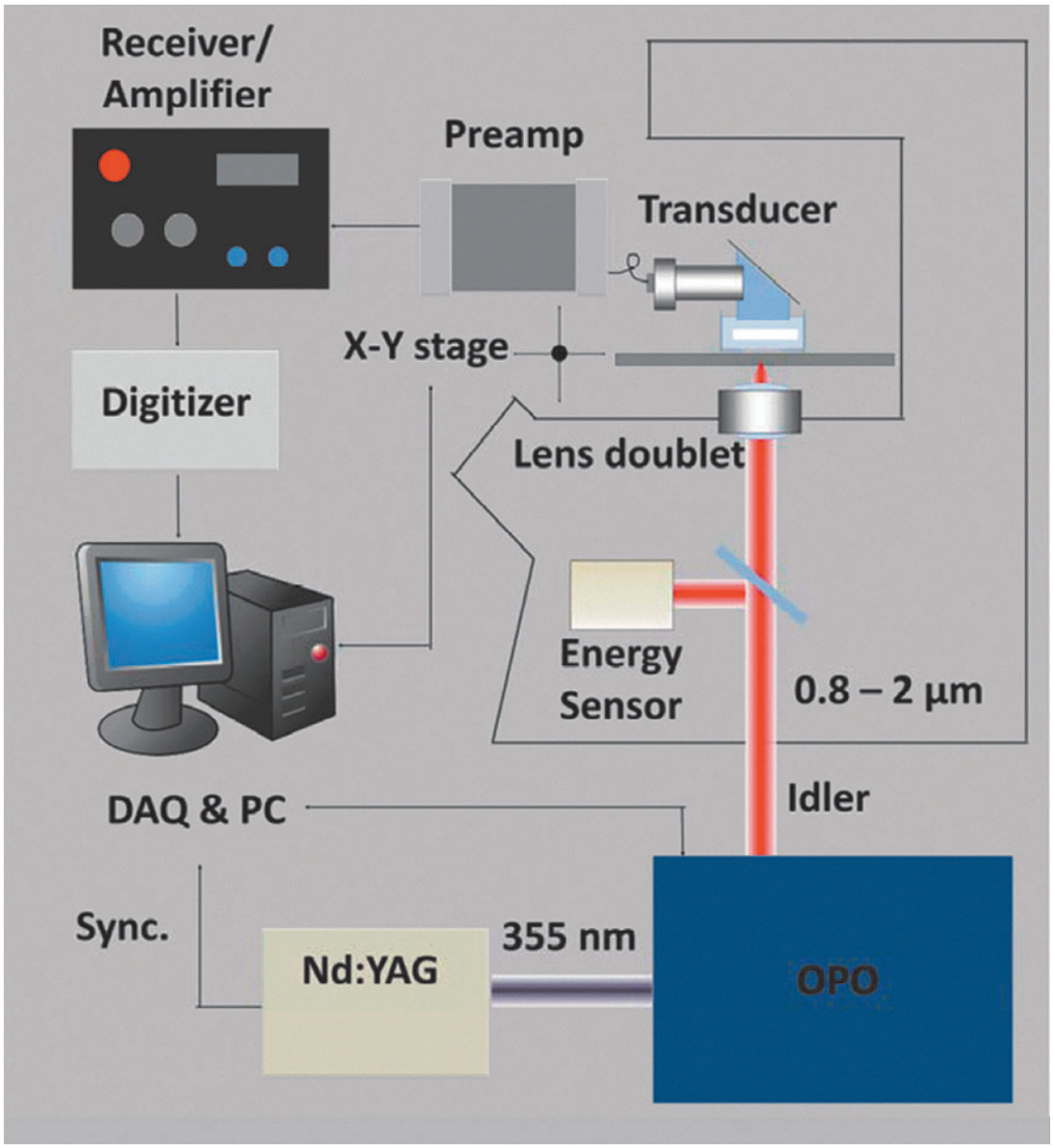

FIG. 1. Schematic of VPA imaging system on an inverted microscope. A Nd:YAG pumped optical parametric oscillator (OPO) produced an idler beam at the wavelength region from 0.8 to 2.0 μm. The excitation was sent to an inverted microscope, and the generated acoustic signal was detected by an ultrasound transducer. The signal was then amplified and sent to a data acquisition system, which is synchronized with the laser pulse. a.u., astronomical unit; DAQ, data acquisition; PC, personal computer. Color image is available online at www.liebertpub.com/neu

days after the injury. In the B-scan PA cross-section image of the injured spinal cord (Fig. 2E), the dorsal portion of the cord (red arrow in Fig. 2E) showed 2 times lower PA signal, compared to the normal spinal cord, indicating a decrease of the CH_2 bond concentration. According to the histology of LFB staining (Fig. 2G–I), an obvious tissue loss in the dorsal WM was visualized at the injury site, consistent with the PA image. The tissue loss may be attributed to myelin degeneration as a result of secondary injury. In the PA image of FA-GC treated spinal cord (Fig. 2F), there was no abrupt PA signal on the dorsal surface of the spinal cord, indicating WM recovery after the treatment. The 3D PA image further confirmed our findings and provided us with additional information on the dimension of the injury (Fig. 2J,K) and FA-GC treatment-mediated recovery (Fig. 2L). Compared to the smooth surface of normal spinal cord, the injured spinal cord showed a clear WM loss on the dorsal surface of the spinal cord (Fig. 2K, enlarged image). Such a loss was prevented after the FA-GC neuroprotective treatment (Fig. 2L). The information was shown in the 3D video as well (Supplementary Video 1) (see online supplementary material at http://www.liebertpub.com). Collectively, these results demonstrated that the PA imaging not only can observe the morphological change before and after injury, but also can assess the efficacy of the neuroprotective medicine on injured spinal cords. The lateral and axial resolution of PA imaging of our system are 10 and 100 μm; but in this study, the lateral resolution is 60 μm, which is limited by the scanning step size and Nyquist's law. Although the

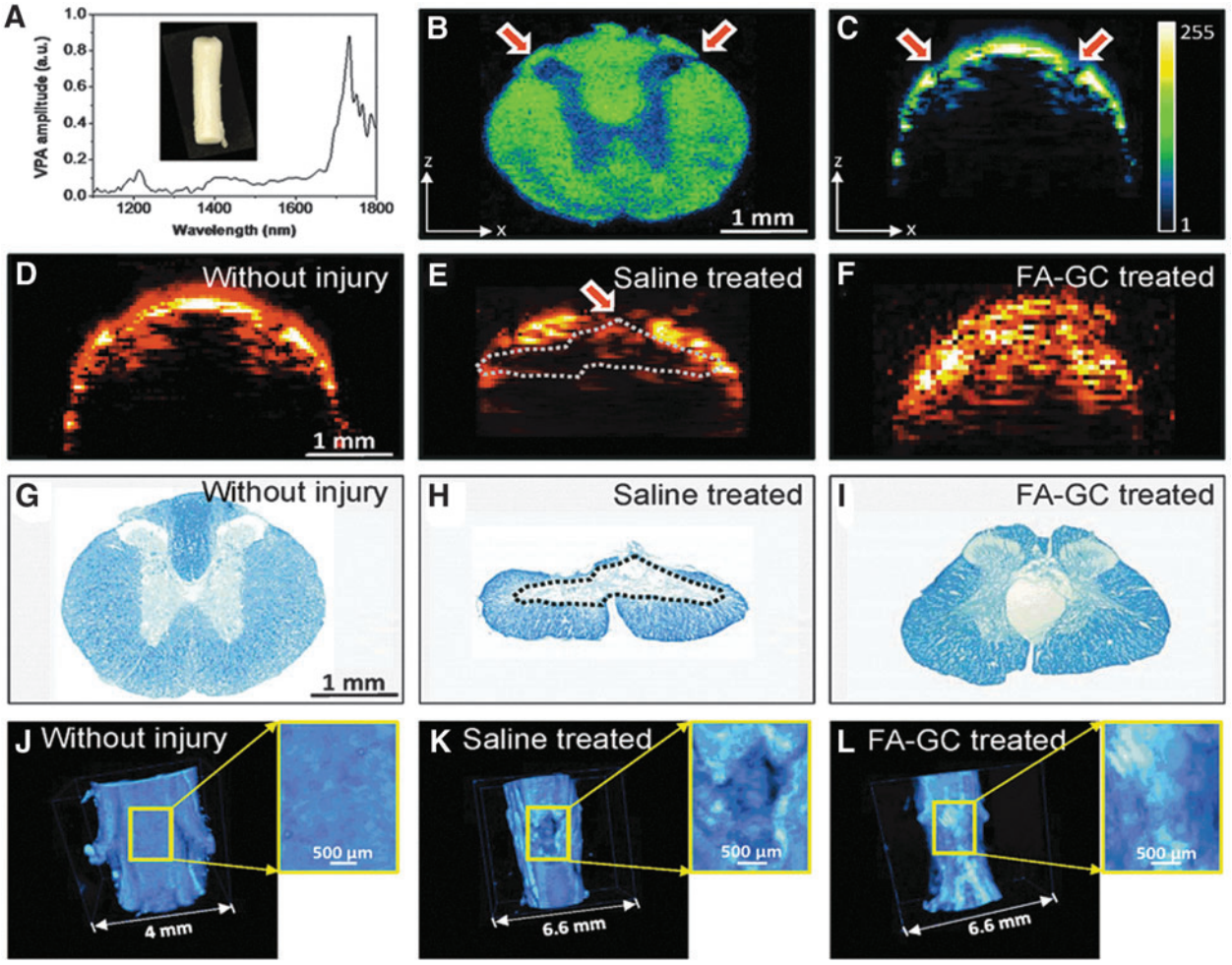

FIG. 2. Photoacoustic (PA) spectra and comparison of spinal cord with/without contusive injury; tissue was harvested at day 28 postinjury. (**A**) PA spectra of white matter of spinal cord. (**B**) PA image of cross-sectioned normal spinal cord. (**C**) B-scan of whole spinal cord without injury. (**D–F**) B-scan PA image of normal spinal cord tissue and of contusive injured tissue with or without treatment. (**G–I**) Luxol fast blue staining of myelin normal spinal cord and in contusive injured spinal cord with or without treatment. (**J–L**) Three-dimensional PA image showing the white matter loss in normal spinal cord and in injured spinal cord with and without treatment. Inset shows the enlarged image of the spinal cord. Dashed lines indicate white matter loss. a.u., astronomical unit; FA-GC, ferulic-acid–conjugated glycol chitosan. Color image is available online at www.liebertpub.com/neu

laser generated heat in spinal cord, no damage to the tissue was observed at this power (less than 1 mW).

In this study, we demonstrated a proof-of-concept novel technology using PA imaging to detect WM loss in rat spinal cord using excitation at 1730 nm. Because the PA signal from CH_2 is capable of distinguishing WM and GM, the WM loss of injured spinal cord can be evaluated. This chemical-selective deep-tissue imaging technique enables the assessment of the WM loss in the spinal cord in a label-free manner, so it offers new opportunities for longitudinal *in vivo* monitoring of the pathology of the spinal cord as well as evaluation of treatment regimens. To conduct *in vivo* imaging in the future, first, we will be using a transducer array, instead of a single-element transducer, to increase the imaging speed up to 2 orders of magnitude; second, we are designing a spinal holder, which will act as a container for the water to facilitate ultrasound transduction and, at the same time, as a stabilizer to immobilize the spine to avoid the vibration caused by breath; and third, a higher-power laser working at 1730 nm is currently being designed and built to achieve a deeper penetration depth in spinal cord.

Acknowledgments

The authors thank Ms. Patti Raley, a medical editor, for her critical reading of the manuscript. This work was supported, in part, by NIH (1R01 NS059622, 1R01 NS050243, and 1R01 NS073636), the Indiana Clinical and Translational Sciences Institute Collaboration in Biomedical/Translational Research Pilot Program Grants (grant no.: RR025761) from the NIH, the Indiana Spinal Cord and Brain Injury Research Foundation, and Mari Hulman George Endowment Funds.

Author Disclosure Statement

No competing financial interests exist.

References

1. Liu, X.Z., Xu, X.M., Hu, R., Du, C., Zhang, S.X., McDonald, J.W., Dong, H.X., Wu, Y.J., Fan, G.S., Jacquin, M.F., Hsu, C.Y., and Choi, D.W. (1997). Neuronal and glial apoptosis after traumatic spinal cord injury. J. Neurosci. 17, 5395–5406.

2. Teng, Y.D., and Wrathall, J.R. (1997). Local blockade of sodium channels by tetrodotoxin ameliorates tissue loss and long-term functional deficits resulting from experimental spinal cord injury. J. Neurosci. 17, 4359–4366.
3. Rosenberg, L.J., Teng, Y.D., and Wrathall, J.R. (1999). Effects of the sodium channel blocker tetrodotoxin on acute white matter pathology after experimental contusive spinal cord injury. J. Neurosci. 19, 6122–6133.
4. Kanellopoulos, G.K., Xu, X.M., Hsu, C.Y., Lu, X., Sundt, T.M., and Kouchoukos, N.T. (2000). White matter injury in spinal cord ischemia: protection by AMPA/kainate glutamate receptor antagonism. Stroke 31, 1945–1952.
5. Wu, W., Wu, W., Zou, J., Shi, F., Yang, S., Liu, Y., Lu, P., Ma, Z., Zhu, H., and Xu, X.M. (2013). Axonal and glial responses to a mid-thoracic spinal cord hemisection in the Macaca fascicularis monkey. J. Neurotrauma 30, 826–839.
6. Liu, N.K., Zhang, Y.P., Titsworth, W.L., Jiang, X., Han, S., Lu, P.H., Shields, C.B., and Xu, X.M. (2006). A novel role of phospholipase A2 in mediating spinal cord secondary injury. Ann. Neurol. 59, 606–619.
7. Peterson, B.J., and Kuhn, R.J. (1965). Some artifacts observed in sections of tissue. Am. J. Clin. Pathol. 43, 235–240.
8. Fulthorpe, J.J., and Cullen, M.J. (1979). Artifacts in tissue-sections. Med. Lab. Sci. 36, 301–302.
9. Kerschensteiner, M., Schwab, M.E., Lichtman, J.W., and Misgeld, T. (2005). *In vivo* imaging of axonal degeneration and regeneration in the injured spinal cord. Nat. Med. 11, 572–577.
10. Huff, T.B., Shi, Y., Sun, W., Wu, W., Shi, R., and Cheng, J.X. (2011). Real-time CARS imaging reveals a calpain-dependent pathway for paranodal myelin retraction during high-frequency stimulation. PloS One 6, e17176.
11. Shi, Y., Zhang, D., Huff, T.B., Wang, X., Shi, R., Xu, X.M., and Cheng, J.X. (2011). Longitudinal *in vivo* coherent anti-Stokes Raman scattering imaging of demyelination and remyelination in injured spinal cord. J. Biomed. Opt. 16, 106012.
12. Wang, P., Wang, H.W., Sturek, M., and Cheng, J.X. (2012). Bond-selective imaging of deep tissue through the optical window between 1600 and 1850 nm. J. Biophotonics 5, 25–32.
13. Wang, H.W., Chai, N., Wang, P., Hu, S., Dou, W., Umulis, D., Wang, L.V., Sturek, M., Lucht, R., and Cheng, J.X. (2011). Label-free bond-selective imaging by listening to vibrationally excited molecules. Phys. Rev. Lett. 106, 238106.
14. Xu, M., and Wang, L.V. (2006). Photoacoustic imaging in biomedicine. Rev. Sci. Instrum. 77, 041101.
15. Gruner, J.A. (1992). A monitored contusion model of spinal cord injury in the rat. J. Neurotrauma 9, 123–126; discussion, 126–128.
16. Ma, P., Liu, H.T., Wei, P., Xu, Q.S., Bai, X.F., Du, Y.G., and Yu, C. (2011). Chitosan oligosaccharides inhibit LPS-induced over-expression of IL-6 and TNF-alpha in RAW264.7 macrophage cells through blockade of mitogen-activated protein kinase (MAPK) and PI3K/Akt signaling pathways. Carbohyd. Polym. 84, 1391–1398.
17. Liu, H.T., Li, W.M., Xu, G., Li, X.Y., Bai, X.F., Wei, P., Yu, C., and Du, Y.G. (2009). Chitosan oligosaccharides attenuate hydrogen peroxide-induced stress injury in human umbilical vein endothelial cells. Pharmacol. Res. 59, 167–175.
18. Liu, H.T., Li, W.M., Huang, P., Chen, W.J., Liu, Q.S., Bai, X.F., Yu, C., and Du, Y.G. (2010). Chitosan oligosaccharides inhibit TNF-alpha-induced VCAM-1 and ICAM-1 expression in human umbilical vein endothelial cells by blocking p38 and ERK1/2 signaling pathways. Carbohyd. Polym. 81, 49–56.
19. Cho, Y., Shi, R.Y., and Borgens, R.B. (2010). Chitosan produces potent neuroprotection and physiological recovery following traumatic spinal cord injury. J. Exp. Biol. 213, 1513–1520.
20. Srinivasan, M., Sudheer, A.R., and Menon, V.P. (2007). Ferulic acid: therapeutic potential through its antioxidant property. J. Clin. Biochem. Nutr. 40, 92–100.
21. Cheng, C.Y., Su, S.Y., Tang, N.Y., Ho, T.Y., Chiang, S.Y., and Hsieh, C.L. (2008). Ferulic acid provides neuroprotection against oxidative stress-related apoptosis after cerebral ischemia/reperfusion injury by inhibiting ICAM-1 mRNA expression in rats. Brain Res. 1209, 136–150.
22. Lin, T.Y., Lu, C.W., Huang, S.K., and Wang, S.J. (2013). Ferulic acid suppresses glutamate release through inhibition of voltage-dependent calcium entry in rat cerebrocortical nerve terminals. J. Med. Food 16, 112–119.
23. Iannotti, C., Ping Zhang, Y., Shields, C.B., Han, Y., Burke, D.A., and Xu, X.M. (2004). A neuroprotective role of glial cell line-derived neurotrophic factor following moderate spinal cord contusion injury. Exp. Neurol. 189, 317–332.
24. Yaroslavsky, A.N., Schulze, P.C., Yaroslavsky, I.V., Schober, R., Ulrich, F., and Schwarzmaier, H.J. (2002). Optical properties of selected native and coagulated human brain tissues in vitro in the visible and near infrared spectral range. Phys. Med. Biol. 47, 2059–2073.

Address correspondence to:
Xiao-Ming Xu, PhD
Spinal Cord and Brain Injury Research Group
Stark Neurosciences Research Institute
Indiana University School of Medicine
320 West 15th Street, NB 500E
Indianapolis, IN 46202

E-mail: xu26@iupui.edu